Geological Magazine

www.cambridge.org/geo

Original Article

Cite this article: Liu H, Liu L, Cao W, Chen Y, and Faure M (2021) Magmatic stock emplacement and its constraints on the localization of related skarn orebodies: an example from the Tongguanshan stock, Tongling district, eastern China. *Geological Magazine* **158**: 2009–2024. https://doi.org/10.1017/S001675682100056X

Received: 28 July 2020
Revised: 12 March 2021
Accepted: 24 May 2021
First published online: 22 July 2021

Keywords:
stock emplacement mechanism; anisotropy of magnetic susceptibility; 3D geometric modelling; Tongling district

Author for correspondence: Liangming Liu, Email: lmliu@csu.edu.cn

CAMBRIDGE UNIVERSITY PRESS

Magmatic stock emplacement and its constraints on the localization of related skarn orebodies: an example from the Tongguanshan stock, Tongling district, eastern China

Hongsheng Liu[1,2], Liangming Liu[1,2], Wei Cao[1,2], Yan Chen[3] and Michel Faure[3]

[1]Key Laboratory of Metallogenic Prediction of Nonferrous Metals and Geological Environment Monitoring, Ministry of Education, Ministry of Education, Changsha, 410083, China; [2]School of Geoscience and Info-Physics, Central South University, Changsha 410083, China and [3]Université d'Orléans, ISTO, CNRS/INSU/BRGM, UMR 7327, 45071 Orléans, France

Abstract

Study of constraints of stock emplacement and geometry on associated skarn orebodies is significant for the understanding of the epithermal deposit system. We have chosen the typical Tongguanshan skarn ore deposit (eastern China) as our target area. The Tongguanshan stock was emplaced at the NE–SW-striking Tongguanshan anticline and is characterized by macroscopically homogeneous quartz–monzodiorite. The magnetic parameters show that the stock is dominated by oblate magnetic ellipsoids and a high degree of anisotropy (> 1.1), and this value is higher at the stock margin. The strike of magnetic foliation at the stock margin is parallel to the stock boundary with sub-horizontal magnetic lineations. A vertical NE–SW-striking magnetic foliation, which is parallel to the regional structures, is revealed inside the stock. The three-dimensional geometric modelling shows that the stock has a tongue-like geometry and the contact surface in both eastern and western sides dips to the NW, but the western side is steeper. Nevertheless, the orebodies are almost developed at the eastern side. Accordingly, we propose that the Tongguanshan stock was constructed by multiple magma pulses, initiated at the SW part of the stock, and ascended along inherited NE–SW extended fractures in the Tongguanshan anticline. The successive magma pulses either accreted by a unilateral E-wards trend or by bilateral magma accretion, which resulted in a deformation difference in the contact zone and caused uneven orebody development. Our study also shows that the strike, dip angle and curvature situation of contact surface, which affects the water–rock reaction process and distribution of the dilation zone, are important ore-controlling factors.

1. Introduction

Skarn orebodies are usually associated with and unevenly developed around magmatic bodies (e.g. Einaudi *et al.* 1981; Baker *et al.* 2004; Meinert, 2005; Mao *et al.* 2011; Sial *et al.* 2011; Xiong *et al.* 2019). It is broadly recognized that the magma composition, oxidation state and degree of fractionation, lithology and structure of country rock will affect the ore genesis process and type of ore deposit (e.g. Einaudi *et al.* 1981; Thompson *et al.* 1999; Audétat *et al.* 2000; Richards, 2003; Baker *et al.* 2004; Meinert, 2005; Seedorf *et al.* 2005). However, the mechanism of localization of intrusion-related orebody is less investigated, which is important to improve understanding of the intrusion-related ore-forming system and further exploitation in the depth (e.g. Ferry & Dipple, 1992; Gerdes *et al.* 1998; Heinrich, 2005; Eldursi *et al.* 2009; Liu *et al.* 2012, 2014).

Previous studies show that the variation of magma composition, temperature and pressure gradient around the magma chamber, permeability and fluid circulation in the contact zone may cause the ore deposition (Ray *et al.* 1995; Audétat *et al.* 2000; Boyce *et al.* 2003; Lu *et al.* 2003; Vallance *et al.* 2003; Matter *et al.* 2005; Eldursi *et al.* 2009; Gerbault, 2012; Luan *et al.* 2014; Gonnermann *et al.* 2017). Nevertheless, this variation is dominantly controlled by the magma emplacement mechanism (e.g. Eldursi *et al.* 2009; Chen & Nabelek, 2017). For example, the gradually emplaced magma injections may accrete in vertical or lateral directions, bilateral or unilateral accretion, and internal filling, which produce different degrees of metamorphism, scale of deformation and fluid circulation patterns in the pluton and contact zone (Scaillet *et al.* 1996; Kratinová *et al.* 2006; Menand, 2008; Tibaldi *et al.* 2007; Paterson *et al.* 2011; Liu *et al.* 2018*a*, 2020). Furthermore, the intrusion-related skarn ore deposit is usually associated with small magmatic bodies (Dines, 1956; Dilles & Proffett, 1995; Tang, 2002). This opinion is well supported by the magmatism–mineralization system in the Tongling district, eastern China (insert in Fig. 1a, b). The Tongling district is characterized by widely developed Lower Cretaceous dioritic stocks (145–135 Ma; Liu *et al.* 2018*b*) that intruded in a NE–SW-striking

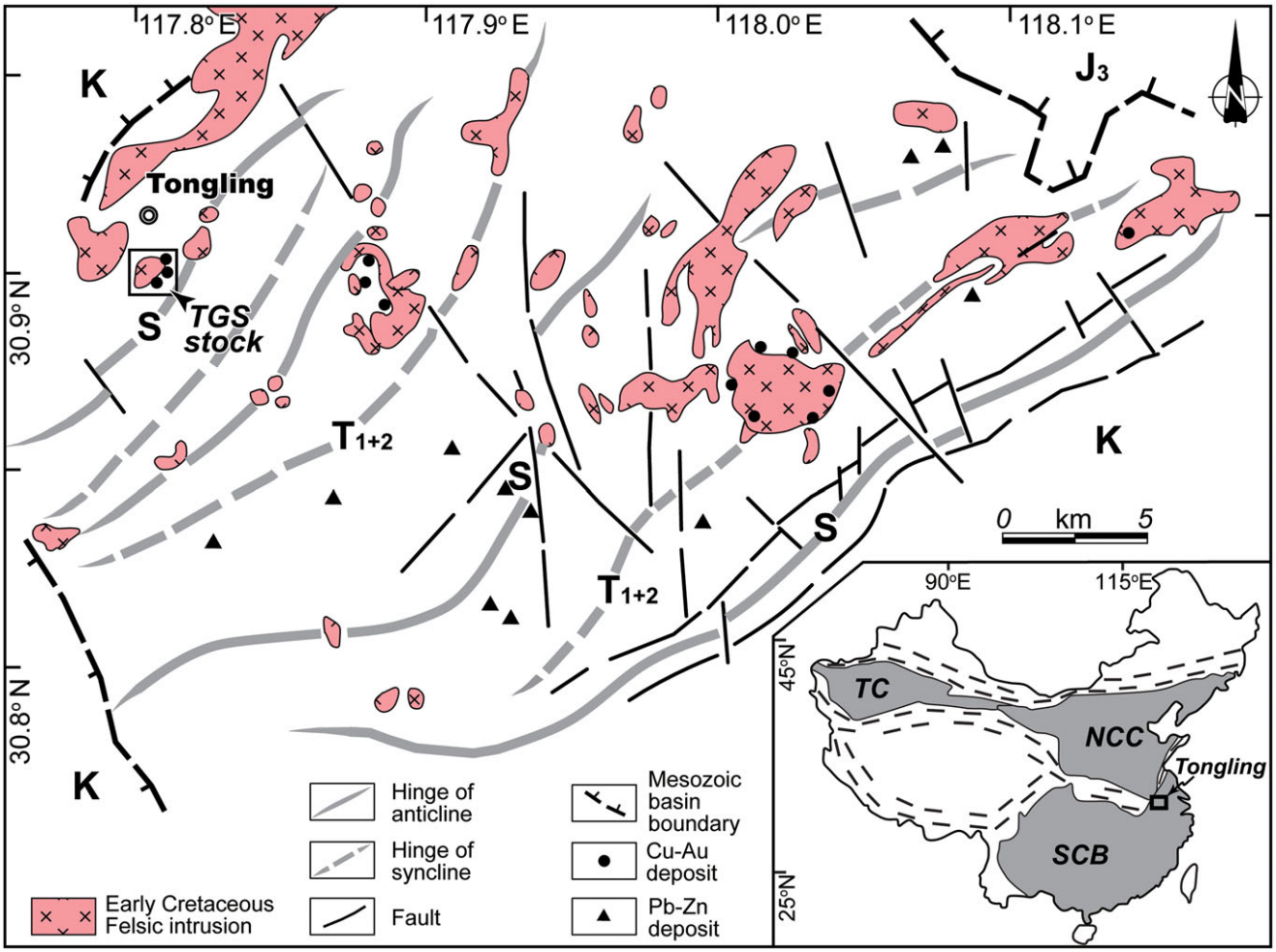

Fig. 1. (Colour online) Tectonic framework of the Tongling district, modified from the 1:50 000 geological map (Geological Team of Anhui Bureau of Geology and Mineral Resources, 1989). K – Cretaceous strata; NCC – North China Craton; SCB – South China Block; S – Silurian strata, T_{1+2} – lower and middle Triassic strata; TC – Tarim Craton.

fold-fault belt in which several world-class skarn-type Cu–Au–Pb–Zn ore deposits have been discovered and mined (Fig. 1b; Chang *et al.* 1991; Pan & Dong, 1999; Wu *et al.* 2013). In contrast, the emplacement of small magmatic bodies, such as stocks, are usually considered as a diapirically emplaced body with instantaneously emplaced magma injection, for example, the La Bazana stock in Iberian Massif (Galadí-Enríquez *et al.* 2003) or the Oulmès stock in Morocco (Tahiri *et al.* 2007). The detailed study of emplacement process of magmatic stock, currently limited, appears to be of major significance in understanding the mechanism of orebody localization in skarn deposits.

The Tongguanshan stock (TGS in Fig. 2; surface area *c.* 1 km^2) is a representative Lower Cretaceous dioritic stock associated with typical skarn and stratabound skarn Cu–Fe–Au deposits developed in the intensively deformed western margin of the Tongling district (Fig. 1b; Pan & Dong, 1999; Mao *et al.* 2011; Li *et al.* 2019). Due to the intensive ore exploration in the Tongguanshan area, detailed geometry of the geological bodies in the depth is well established and therefore provides an excellent base from which to understand the stock emplacement processes and evaluation of the relationship between the stock emplacement and skarn mineralization. The Tongguanshan stock was therefore chosen as our target to reveal how the stock emplacement controls the localization of associated skarn-type ore deposits. We conducted detailed macro- and microscopic structure and fabric investigations, anisotropy of magnetic susceptibility (AMS) and three-dimensional (3D) geometric modelling on the Tongguanshan stock and its related orebodies, acquiring new constraints on the stock emplacement process and the associated orebody.

2. Geological background

The Tongling district, located at the eastern margin of China mainland, is characterized by widely developed Lower Cretaceous dioritic stocks with surface area ranging over *c.* 0.5–20 km^2 (Fig. 1). The Early Cretaceous magmatism in the Tongling district can be classified into two main series, namely the high-K, calc-alkaline series and the shoshonitic series, related to the typical skarn-type Cu-Fe and Au deposits, respectively (Fig. 1; Chang *et al.* 1991; Li *et al.* 2007; Xie *et al.* 2008; Liu *et al.* 2010, 2014; Deng *et al.* 2011; Wu *et al.* 2013). The Tongling district was highly deformed by pre-Cretaceous tectonic events since Neoproterozoic time, including the Neoproterozoic collision between the Yangtze and Cathaysia blocks, the late Neoproterozoic South China block rifting, the Palaeozoic and early Mesozoic intracontinental events, and the Early Cretaceous compression and extension events, producing the current major series of NE–SW-striking S-type fold system (Fig. 1; e.g. Wang & Li, 2003; Hacker *et al.* 2004; Xu *et al.* 2006;

https://doi.org/10.1017/S001675682100056X Published online by Cambridge University Press

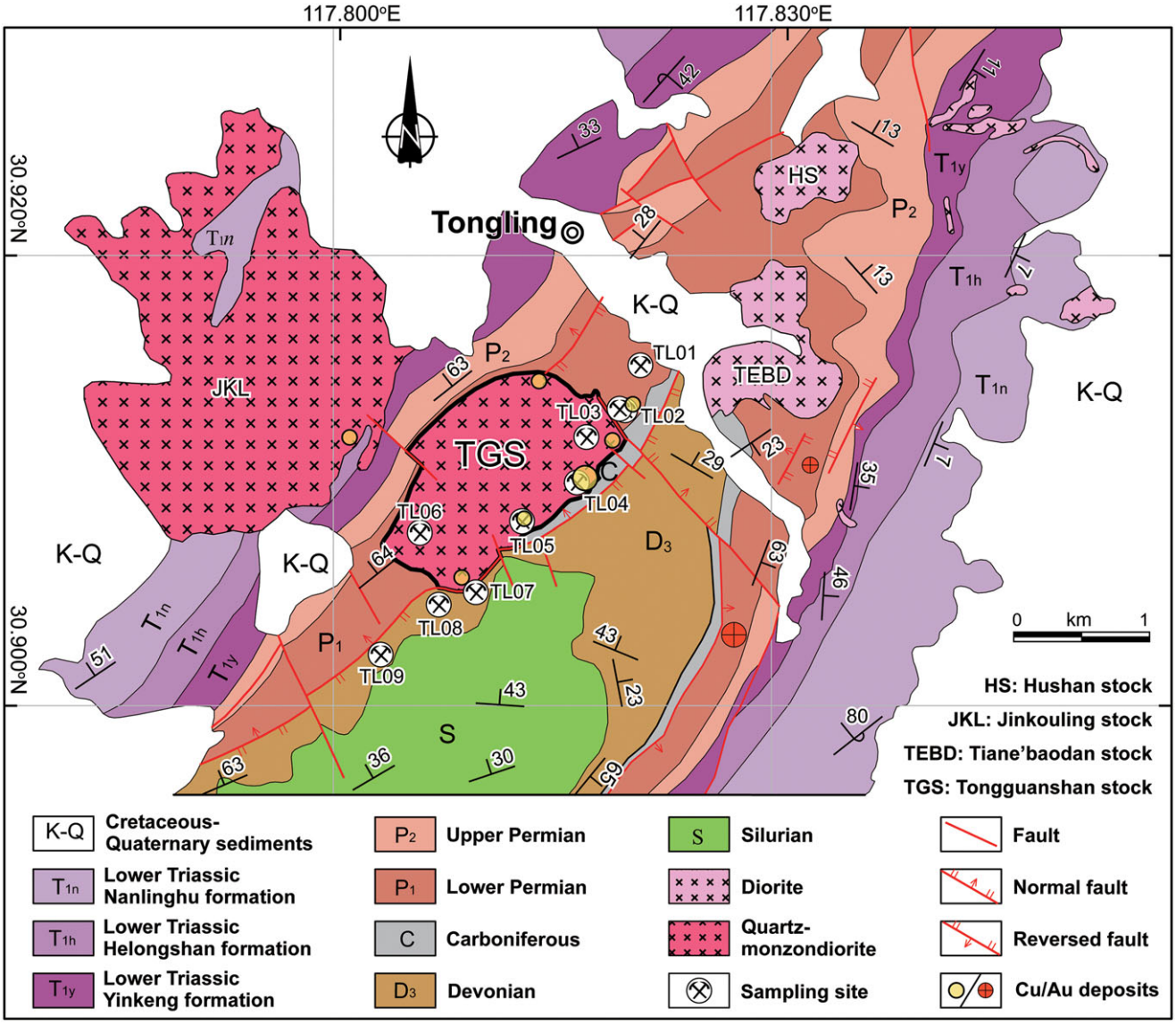

Fig. 2. (Colour online) Geological map of the Tongguanshan ore field (according to the 1:50 000 geological map (Geological Team of Anhui Bureau of Geology and Mineral Resources, 1989).

Faure *et al.* 2009; Deng *et al.* 2011; Shu *et al.* 2011). Due to the rigidity difference and differential deformation developed at the brittle crust level, there are some saddle-like weak zones existing in the core of the anticline. The E–W-trending basement faults were also revealed by the geophysical studies (Lü *et al.* 2003), the activation of which during the early Mesozoic epoch produced the NW-trending faults (Fig. 1; Deng *et al.* 2006). The intersection of these NE-, NW- and EW-trending faults facilitate the magma ascent and emplacement.

The Tongguanshan stock is an Early Cretaceous quartz–monzodioritic stock (141.8 ± 1.0 Ma; Wu *et al.* 2010), intruded in the western limb and hinge of the NE–SW-striking Tongguanshan anticline (Figs 1, 2), and displays a roughly oval-shaped exposure of *c.* 1 km^2 with its long axis parallel to the hinge of the Tongguanshan anticline (Fig. 2; Wang *et al.* 2004; Xu *et al.* 2004; Du *et al.* 2007; Xie *et al.* 2008; Wu *et al.* 2010). Macroscopically, the Tongguanshan stock is an isotropic monzodioritic body mainly composed of medium- to fine-grained quartz–monzodiorite without any obvious lithological or textural zonation (Fig. 3a). Dioritic enclaves are irregularly shaped and weakly oriented, with long axes parallel to the regional structures or the stock–country-rock boundary. Previous geobarometric studies on the Tongguanshan stock and the surrounding contemporaneous Tiane'baodan stock (TEBD in Fig. 2) have similar emplacement depths at *c.* 3–5 km (Du *et al.* 2004; Cao *et al.* 2009; Lei *et al.* 2010). Numerous NE–SW-striking garnet-bearing veins, dipping to the SE and parallel to the regional structures, are developed in the eastern margin of the Tongguanshan stock (Fig. 3b, c).

The country rocks of the Tongguanshan stock mainly consist of Permian limestone and siltstone in its western side, and Carboniferous limestone–dolomite strata and Devonian sandstone in its eastern side (Fig. 2). The Devonian strata are dominated by the Wutong group, which possess the highest rigidity among these country rocks (Deng *et al.* 2006). In the northern part of the stock (site TL01 in Fig. 2), the bedding of Permian limestone strikes NE–SW and dips to the NW at *c.* 50° with weak recrystallization of the limestone (Fig. 4a). Moreover, according to the field survey in the Tongguanshan orefield, the lower Permian strata in its NE margin

https://doi.org/10.1017/S001675682100056X Published online by Cambridge University Press

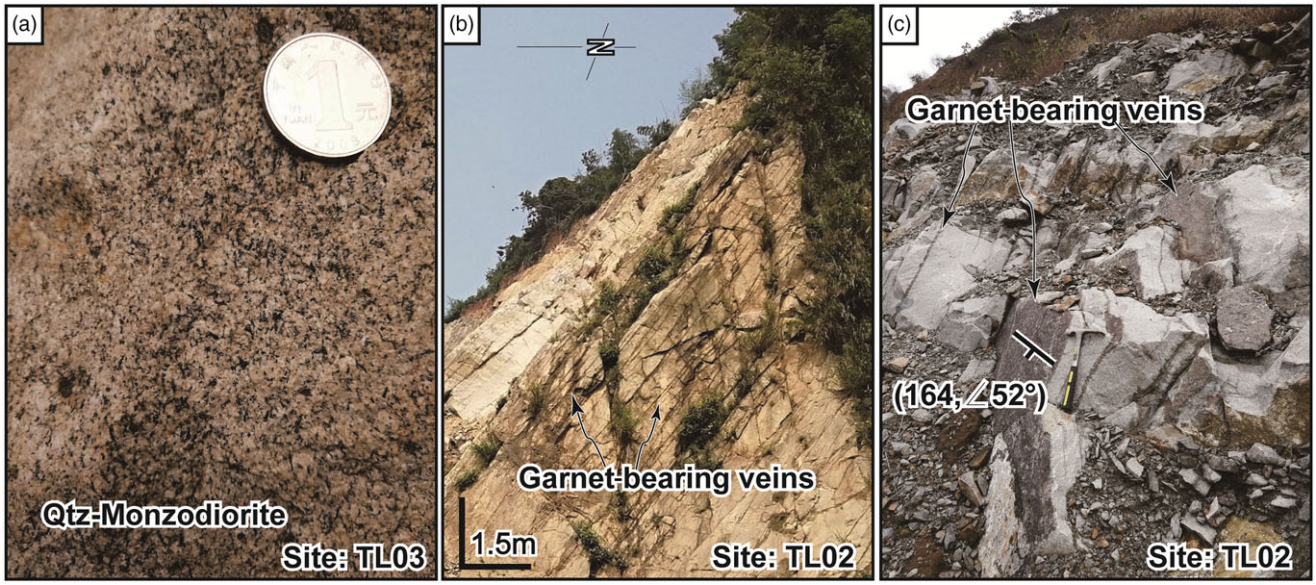

Fig. 3. (Colour online) (a) Field observations of the Tongguanshan stock, (b) quartz–monzodiorite of the stock and (c) garnet-bearing veins developed in the NE margin of the stock.

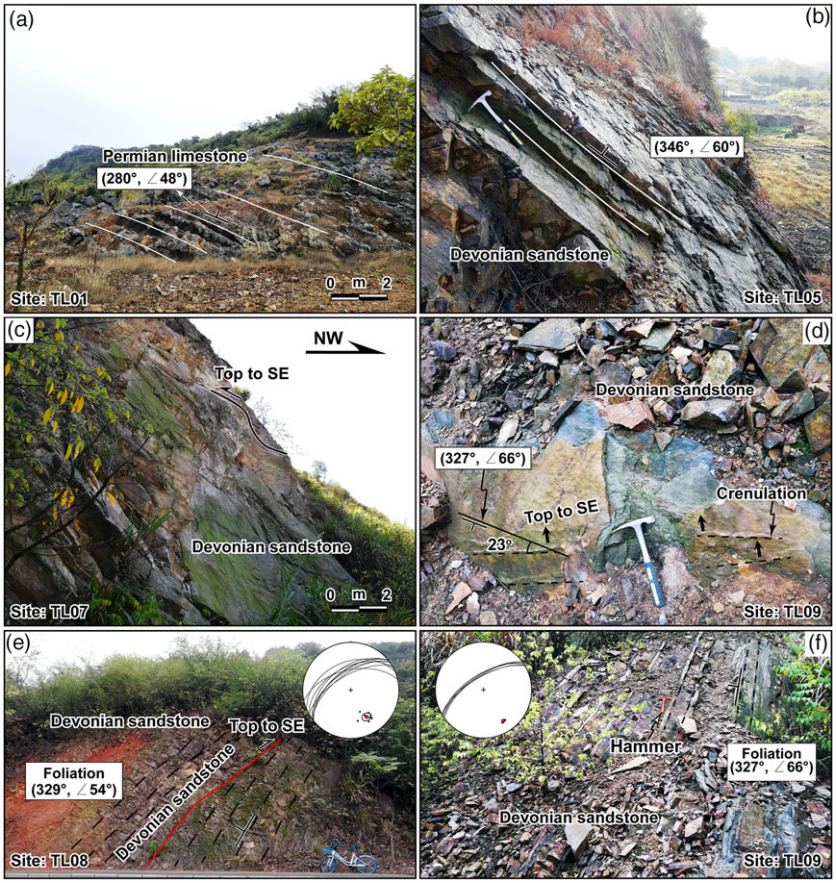

Fig. 4. (Colour online) Field observations of the country rocks of the Tongguanshan stock: (a) bedding of the Permian limestone in the northern stock margin; (b, c) Devonian sandstone country rocks along the contact; and (d–f) Devonian sandstone of the country rock with certain distance to the stock, equal-area projection of the bedding of the strata inserted.

are folded (Fig. 5). In the SE part of the Tongguanshan stock, the hornfels-facies Devonian sandstone is well preserved and exposed in the thermal aureole (i.e. sites TL05, TL07, TL08 and TL09 in Fig. 2). The bedding of the Devonian sandstone presents consistent NE–SW strikes with dip angles varying over 54–66° (Fig. 4b–f). Moreover, the folds of the Devonian strata developed along the contact zone show SE vergence (Site TL07 in Fig. 4c). Similar structures are also recorded in the sites far away from the stock, for example, the crenulation of shale (Fig. 4d) and thrust (Fig. 4e) can be observed at sites TL08 and TL09, respectively. These

https://doi.org/10.1017/S001675682100056X Published online by Cambridge University Press

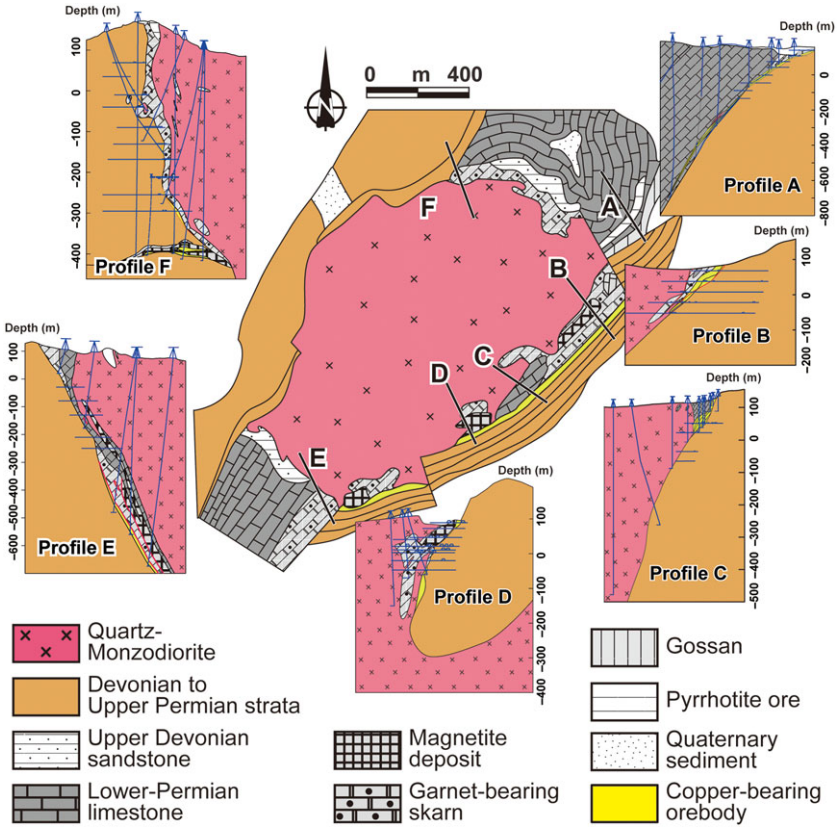

Fig. 5. (Colour online) Representative cross-sections along the Tongguanshan stock, according to the drilling data.

consistent kinematic indicators were revealed in and far away from the stock–country-rock contact zone, suggesting that the country rocks had suffered a top-to-SE thrusting before the magma emplacement. However, due to the urbanization on the western side of the stock, no available country rocks and stock exposures can be observed on the surface.

The Tongguanshan stock is also characterized by voluminous skarn-type copper deposits, which are dominantly located in the northeastern, eastern and southeastern parts of the stock, and the orebodies are mainly developed in the contact zones with strikes parallel to the contact surface, as well as the regional structures (Fig. 5). According to Meng *et al.* (2004) the age of mineralization is 135.48 ± 0.45 Ma in the Tongguanshan stock, that is, subsequent to the stock emplacement (*c.* 140 Ma; Wu *et al.* 2010). Six representative profiles around the Tongguanshan stock revealed by the drilling data are presented in Figure 5, showing that the inward dip angles of the contact surface gradually decrease from *c.* 75° in the south (profile E in Fig. 5) to *c.* 40° in the north (profile A in Fig. 5).

3. Methodology and sampling

3.a. Petrofabric observation

As mentioned above, our field survey shows that no obvious emplacement-related fabrics can be observed in the Tongguanshan stock; we therefore conducted detailed microscopic petrofabric studies by thin-section observation and anisotropy of magnetic susceptibility (AMS) analysis to acquire a better understanding of its emplacement process. We collected five samples (TL05-D, TL07, TL08, TL09A and TL09B; Table 1 and Fig. 2), oriented by both magnetic and solar compasses, from the country rocks and prepared them for microscopic fabric and kinematic investigations. The samples were cut along the XZ plane, that is, perpendicular to the foliation and parallel to the lineation. One massive quartz–monzodiorite sample was also collected at site TL06 for thin-section investigation (Fig. 2).

3.b. Anisotropy of magnetic susceptibility

Being an efficient method for fabric investigation, AMS has been widely applied on magma emplacement studies in South China (Feng *et al.* 2012; Wei *et al.* 2014, 2016; Ji *et al.* 2018; Liu *et al.* 2018*a*). In the Tongling district, the AMS was also applied on the contemporaneous Fenghuangshan pluton to reveal its emplacement process (Zhang *et al.* 2008). As the western part of the Tongguanshan stock is inaccessible due to extensive urbanization, only four fresh outcrops in the eastern side of the stock were collected, that is, samples TL02, TL03, TL04 and TL05 (Fig. 2 and Table 2). At least seven oriented core samples were collected at each site using a portable gasoline drill. The raw core samples were cut into standard cylindrical specimens of length 2.2 cm and diameter 2.5 cm, respectively. Finally, 64 specimens were prepared for the AMS measurement. Before the measurement, the orientation of the cores without solar compass measurement was corrected by –4.2°, that is, the average of azimuth differences between magnetic and solar azimuths.

Our AMS measurements and magnetic mineralogy experiments were conducted in the Paleomagnetism Laboratory of Nanjing University. The core samples and rock powders were analysed by the KLY-3S Kappabridge coupled with the CS3 furnace of AGICO Company. Protective argon gas was added to reduce the oxidation during the heating process. The AMS data were calculated with the open access software ANISOFT of AGICO

https://doi.org/10.1017/S001675682100056X Published online by Cambridge University Press

Table 1. Country rock samples collected from the Tongguanshan area

Sample	Geographic coordinates	Lithology	Observations
TL05D	30.9058° N, 117.8105° E	Hornfel sandstone	Bedding of the Devonian sandstone (346°, ∠ 60°) and parallel with the granite–country-rock contact
TL06	30.9072° N, 117.8018° E	Quartz–monzodiorite	Undeformed with dark minerals up to 60%
TL07	30.9028° N, 117.8060° E	Sandstone	Weakly hornfel sandstone and folding of the bending is observed
TL08	30.9009° N, 117.8021° E	Sandstone	Thick Devonian sandstone (*c.* 30 cm) alternates with thin siltstone layers; bedding of this sequence is *c.* 329°, ∠ 54° and cut by the top-to-SE thrust
TL09A	30.899° N, 117.8003° E	Shale	Fine-grained Devonian sandstone and siltstone layers with bedding occurrence of 327°, ∠ 66° with crenulation observed in thin layered siltstone
TL09B	30.899° N, 117.8003° E	Siltstone	Fine-grained Devonian sandstone and siltstone layers with bedding occurrence of 327°, ∠ 66° with crenulation observed in thin layered siltstone

Table 2. Sampling information and site-mean anisotropy of magnetic susceptibility measurement results for the Tongguanshan stock. Lithology: quartz–monzodiorite

Site	Location	Altitude (m)	No. specimens	Bulk magnetic susceptibility (K_m, dimensionless)	Degree of susceptibility anisotropy (P_J)	Shape parameter of ellipsoid (T)	Magnetic lineation (K_1)		Pole of magnetic foliation (K_3)	
							Declination/inclination (°)	α_{95} (max/min) (°)	Declination/inclination (°)	α_{95} (max/min) (°)
TL02	30.9137° N, 117.8173° E	75	22	37300	1.17	0.005	331.2/27.1	6.6/4.2	72.2/20.6	7.9/3.9
TL03	30.9104° N, 117.8147° E	112	14	50600	1.09	0.410	28.3/42.6	81.0/12.3	295.9/2.6	17.6/11.3
TL04	30.9084° N, 117.8137° E	95	12	30800	1.13	0.430	342.9/37.3	36.4/3.7	119.7/43.7	9.6/5.7
TL05	30.9058° N, 117.8105° E	100	16	52900	1.37	0.070	251.7/4.3	12.3/6.9	160.9/10.7	7.4/4.1

$K_m = (K_1 + K_2 + K_3)/3$; $P_J = \exp(\{2[(n_1 - n)^2 + (n_2 - n)^2 + (n_3 - n)^2]\}^2)$, $T = (2n_2 - n_1 - n_3)/(n_1 - n_3)$, where n_1, n_2 and n_3 are the natural-logarithm-normalized susceptibilities K_1, K_2 and K_3, respectively.

Company. Site-mean directions are calculated from the three principal axes of the magnetic ellipsoid ($K_1 \geq K_2 \geq K_3$) with 95% confidence level, where K_1 and K_3 correspond to the magnetic lineation and pole of the magnetic foliation, respectively. Detailed explanations of the magnetic parameters are provided in Table 2. Ten cylindrical quartz–monzodiorite specimens (TL02-7B, TL02-9, TL03-2, TL03-7, TL04-2A, TL04-7, TL05-1, TL05-5, TL05-10 and TL05-13) were chosen for the oriented thin-section study, and were cut along the XZ plane, that is, perpendicular to the magnetic foliation and parallel to the magnetic lineation.

3.c. Geometric modelling of the Tongguanshan stock and its related orebodies

The recognition of the geometry of the Tongguanshan stock and its related ore bodies is pivotal to the understanding of its emplacement process, as well as the relationship between the magma emplacement and the related mineralization. However, considering its small size and complexity, as well as the surrounding intensive human activities, traditional geophysical investigation methods in this area are less efficient in determining the stock geometry. To determine the 3D geometry of the geological bodies, we therefore acquired a high-resolution digital elevation model (DEM), drilling data and regional resistivity surveying data from the Tongling Nonferrous Metals Group Holdings Company, and combined these with our structure and petrofabric investigation results in the Tongguanshan area (Table 3). We integrated and processed these data using Micromine 2014 (https://www.micromine.com/) to reconstruct the 3D surface of the geological bodies. First, the contacts of the geological bodies in the depth were digitalized from the borehole profiles. Second, outlines of adjacent contacts between similar geological units were connected using a triangulated irregular network (TIN) to obtain the contact surface. Third, the contact surface was smoothed using a discrete smooth interpolation (DSI) to approximate the real geological interface. The method for the reconstruction of the 3D geometry of the geological bodies is reported in detail by Liu *et al.* (2012).

4. Results

4.a. Petrofabric investigation of the Tongguanshan stock and its country rocks

According to our thin-section observation, the quartz–monzodiorite of the Tongguanshan stock is composed of plagioclase, K-feldspar, quartz, hornblende, sphene, biotite, apatite, pyrrhotite and magnetite (Fig. 6). Most of the samples present a similar magmatic texture and euhedral mineral with grain sizes ranging from 0.5 to 1.5 mm, but weak orientation in the mineral long axis direction can

https://doi.org/10.1017/S001675682100056X Published online by Cambridge University Press

Table 3. Data compilation for 3D geometric modelling

Data type	Quantity	Objectives	Data source
Geological and digital elevation model (DEM)	1 sheet	Define the boundary of different geological units on the surface	Tongling Nonferrous Metals Group Holding Company
High-resolution remote sensing image	1 sheet	Searching for outcrops in the surface	Central South University
Prospecting profile map	172 sheet	Obtain the contact of different geological units in the depth	Tongling Nonferrous Metals Group Holding Company
Borehole survey, core logging and sample analysis	447 borehole with 99 812 m core data and 9120 specimens for ore grade analysis	Acquire the contact of different geological units in the area without borehole data, and the ore grade variation	Tongling Nonferrous Metals Group Holding Company
Controlled source audio-frequency magnetotellurics (CSAMT)	441 surveying points with 9475 resistivity surveying data	The variation of the resistivity in the depth, to better constrain the contact of different geological units	Central South University

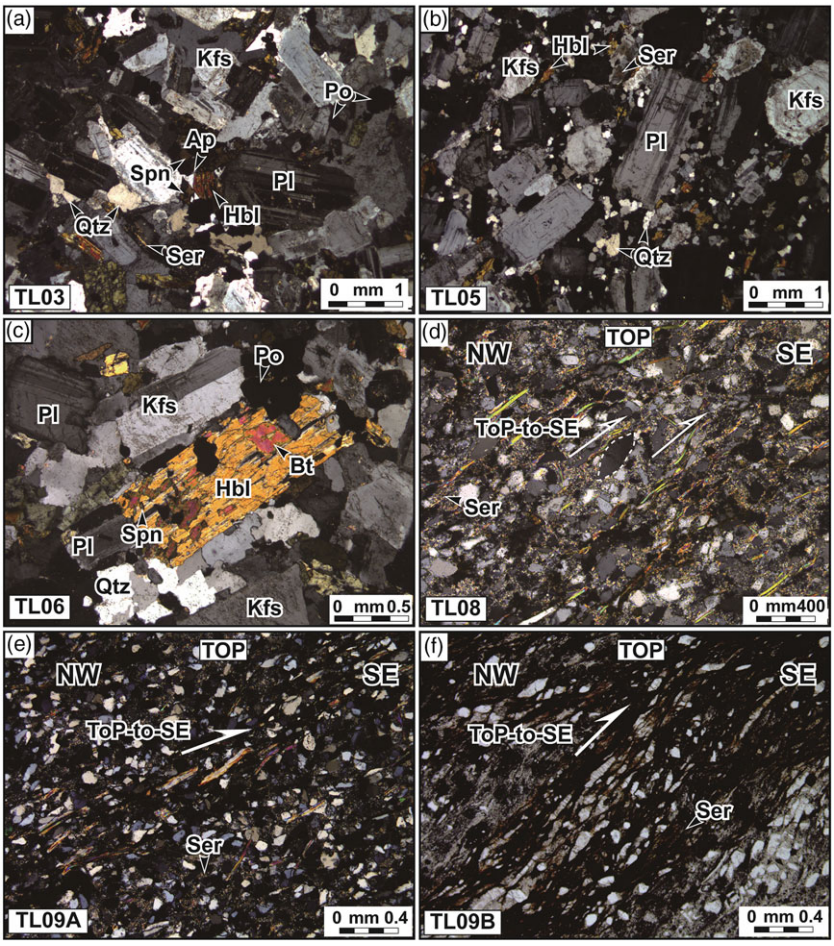

Fig. 6. (Colour online) (a–c) Thin-section observations of the quartz–monzodiorite of the TGS stock and (d–f) thin-section observations of the country rocks with indicated kinematic information. Ap – apatite; Bt – biotite; Hbl – hornblend; Kfs – K-feldspar; Pls – plagioclase; Po – pyrrhotite; Spn – sphene.

be observed (Fig. 6a–c). Nevertheless, sample TL05, located in the contact zone and characterized by fine-grained and irregular grain boundary of the quartz and feldspar (Fig. 6b), shows a grain boundary migration recrystallization, probably a result of the interaction with the country rocks during the magma emplacement. No consistent sub-solidus deformation fabrics were identified in the quartz–monzodiorite.

Country-rock samples TL05D and TL07 collected in the contact zone are characterized by homogeneous clastic texture and strong thermal alteration; these samples are not suitable for kinematic study because of their fine-grained mineral size. The other three samples of sandstone (TL08, TL09A and TL09B; Fig. 2), collected from south of the Tongguanshan stock and on the western limb of the Tongguanshan anticline, have similar clastic texture with clast grain

https://doi.org/10.1017/S001675682100056X Published online by Cambridge University Press

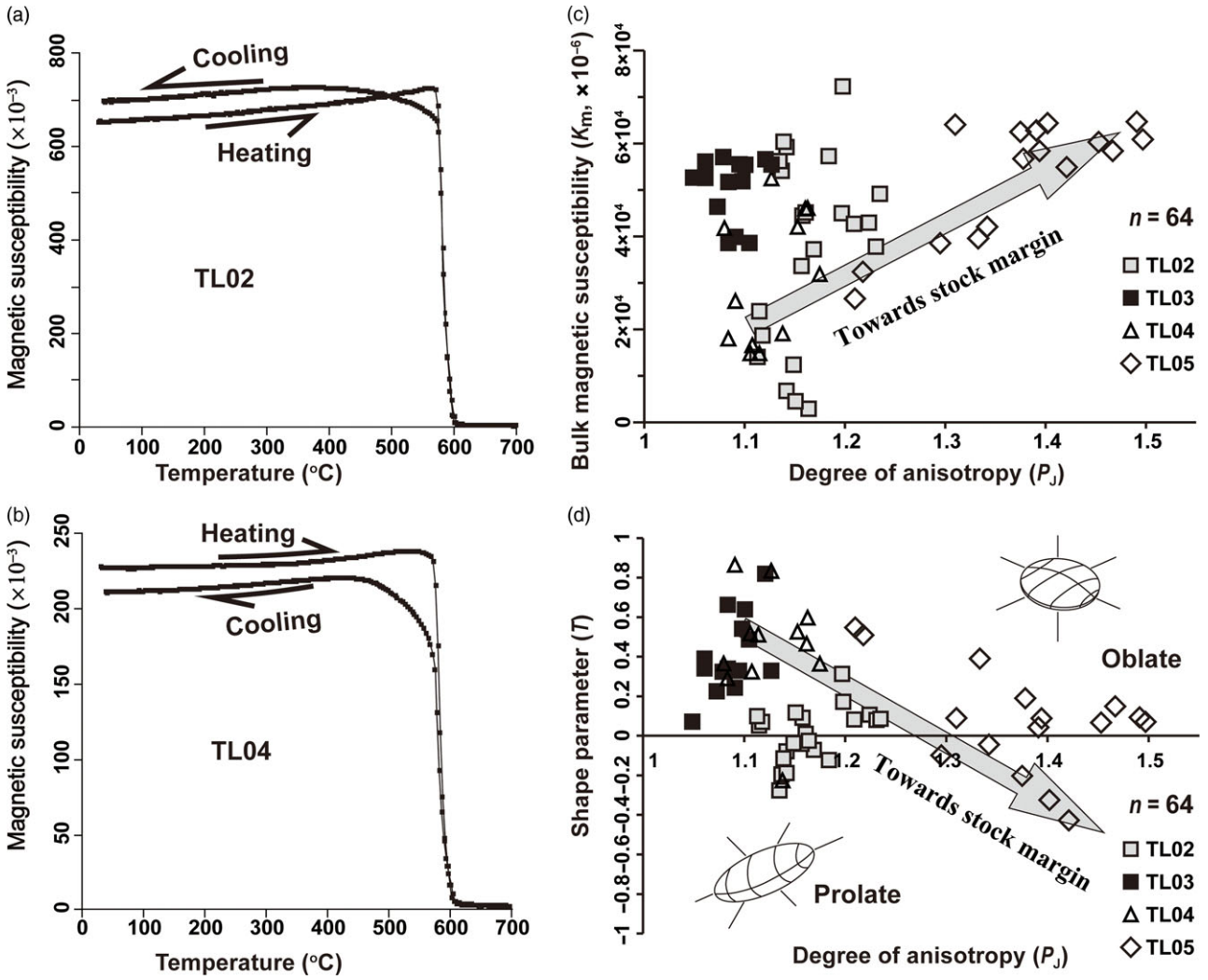

Fig. 7. (a, b) Representative magnetic mineralogy investigation and (c, d) magnetic parameters of the Tongguanshan stock quartz–monzodiorite.

sizes of *c.* 100 μm (Fig. 6d–f), and the foliation is well defined by the oriented biotite and muscovite grains. We observed 'sigmoidal' plagioclase and quartz grains (Fig. 6d–f) and 'bookshelf' mica grains (Fig. 6e), suggesting a top-to-SE movement. These phenomena further confirm that the western limb of the Tongguanshan anticline experienced a top-to-SE movement before the stock emplacement. No high-grade metamorphic minerals were identified in the country rocks.

4.b. Magnetic fabrics

4.b.1. Magnetic mineralogy analysis

A total of eight specimens were milled for the thermal magnetic mineral analysis and present similar curves of magnetic susceptibility (k) versus temperature (T); we therefore only depict two representative k–T curves in Figure 7a and b. The heating curves display a slight increasing of magnetic susceptibility during the heating process, and a rapid drop to zero at 580 °C, suggesting that the magnetite is the major magnetic susceptibility carrier in the Tongguanshan quartz–monzodiorite. The lack of Hopkinson peak in these curves suggests that the magnetite is dominated by samples of a multidomain nature (Dunlop, 1974). This interpretation is also supported by the relatively high site-mean bulk magnetic susceptibility of the quartz–monzodiorite, ranging from *c.* 31 to 53 × 10^{-3} (Table 2). Accordingly, the magnetite is the dominant contributor to the magnetic fabric of the quartz–monzodiorite in the Tongguanshan stock. We calculated K_1 and K_3 of the magnetic ellipsoid for the magnetic lineation and pole of magnetic foliation, that is, the AMS result corresponding to a normal petrofabric.

4.b.2. Features of the magnetic parameters

Most of the measured specimens show a degree of anisotropy (P_J) greater than 1.1 (Fig. 7c; Table 2), and these high values may be related to the high concentration of magnetite as opposed to the post-emplacement deformation (Rochette *et al.* 1992). The preferred orientation of magnetic minerals, which is another cause of degree of anisotropy, may be due to the magma flow or interaction between magma and country rocks. Values of P_J are higher in the sites located closest to the stock–country-rock contact (Fig. 7c), implying that high values of P_J may be due to the result of the interaction between magma and country rocks. The shape parameter (T), representing the shape of the magnetic susceptibility ellipsoid, is divided into two groups: oblate ($0 < T < 1$) and prolate ($-1 < T < 0$). The majority of the specimens are located in the

https://doi.org/10.1017/S001675682100056X Published online by Cambridge University Press

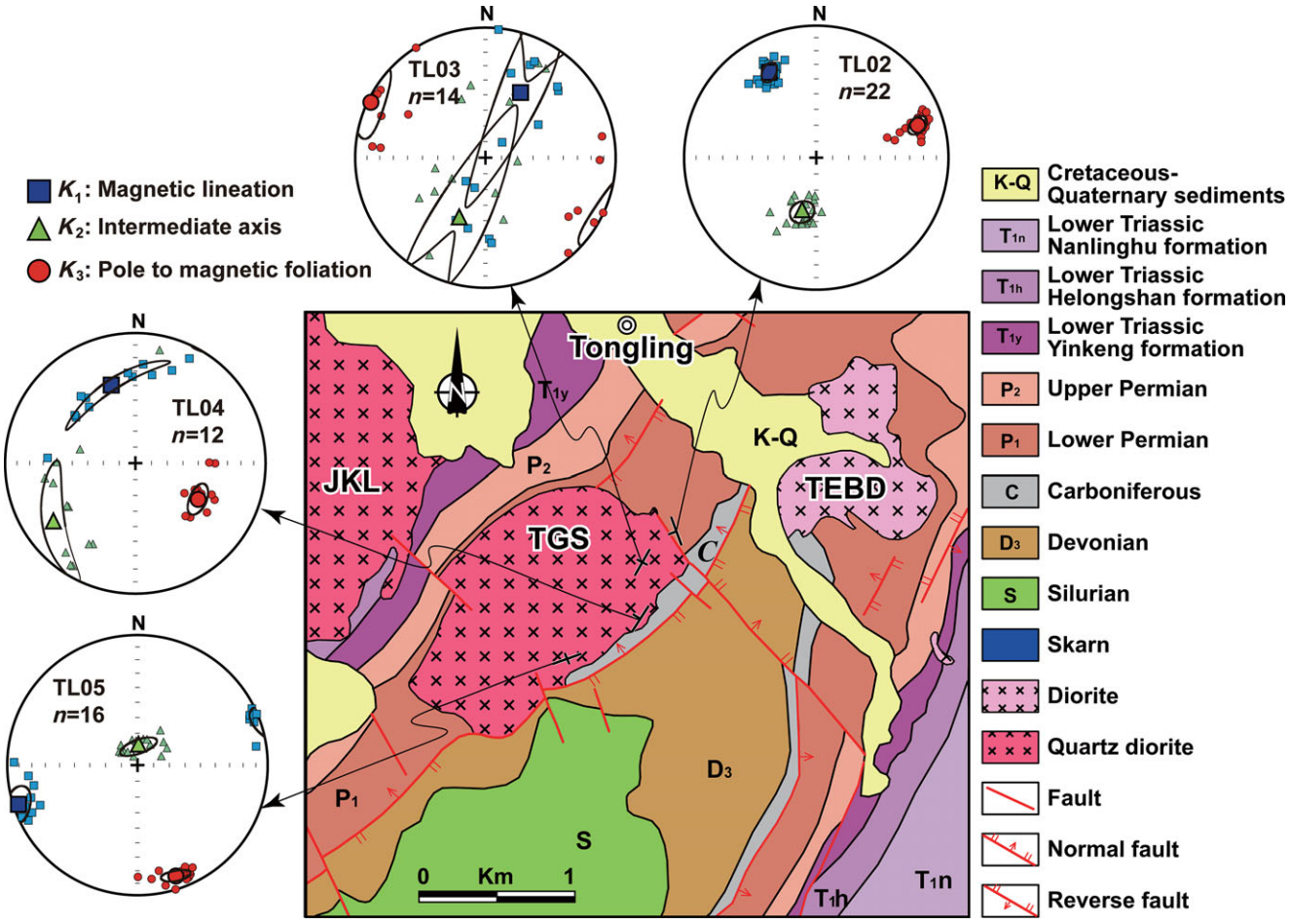

Fig. 8. (Colour online) AMS Tongguanshan stock results.

oblate domain (Fig. 7d; Table 2), implying that the planar fabric is better developed than the linear fabric.

4.b.3. AMS of the Tongguanshan stock

We present the AMS results by equal-area projections (lower hemisphere) with the three principal axes, site-mean value and 95% confidence level (Fig. 8; Table 2). The sites near the margin of the stock (i.e. TL02, TL04 and TL05) are characterized by well grouped inwards-dipping and sub-vertical to vertical (45–80°) magnetic foliations with strikes parallel to the stock boundary (Fig. 8). The magnetic lineations of these sites, which may record the trend of magma flow, are horizontal to sub-horizontal (Fig. 8; Table 2). However, site TL03 (*c.* 200 m to the stock boundary) presents vertical NE–SW-striking magnetic foliations parallel to the regional structures; however, the magnetic lineations show variable plunges (Fig. 8).

4.c. Stock geometry and the occurrence of the orebodies

By detecting the contact surface from the drilling profiles and 3D modelling, we can build the geometry of the Tongguanshan stock in the depth (Fig. 9). Several features are highlighted in our 3D geometric model. First, the shape of the contact boundary in the eastern side is much more complicated than in the western side (Fig. 9a). Second, the Tongguanshan stock has a tongue-like geometry with a sharp wedge out at –2 km (dashed line in Fig. 9b). We therefore estimate the volume of the Tongguanshan stock as *c.* 1.25 km^3. Third, the stock–country-rock contact surface generally dips to the NW in both east and west sides with dip angle steepening when moving to the depth, and is steeper in the west side than in the east side (Fig. 9c). Fourth, the orebodies are mainly located in the east side of the stock and the highest reservation is revealed in the NE margin. The extent of the orebodies is roughly parallel to the stock–country-rock contact surface.

5. Discussion

5.a. Emplacement mechanism of the Tongguanshan stock

5.a.1. Implications of the petrofabrics for the magma emplacement

Our field and microscopic observations revealed that the Tongguanshan stock has a macroscopically isotropic appearance. Although the values of degree of anisotropy are mainly > 1.1, probably because of the high concentration of magnetite (Fig. 7d), no sub-solidus deformation has been identified in the stock and its country rocks. We therefore propose that the Tongguanshan stock has not experienced a strong post-emplacement deformation related to a regional tectonic event. As a result, the magnetic fabrics developed in the stock are primary and reflect the magma emplacement process and the interaction between the magma and its country rocks, and the magnetic lineation may indicate the magma flow direction (Rochette *et al.* 1992).

https://doi.org/10.1017/S001675682100056X Published online by Cambridge University Press

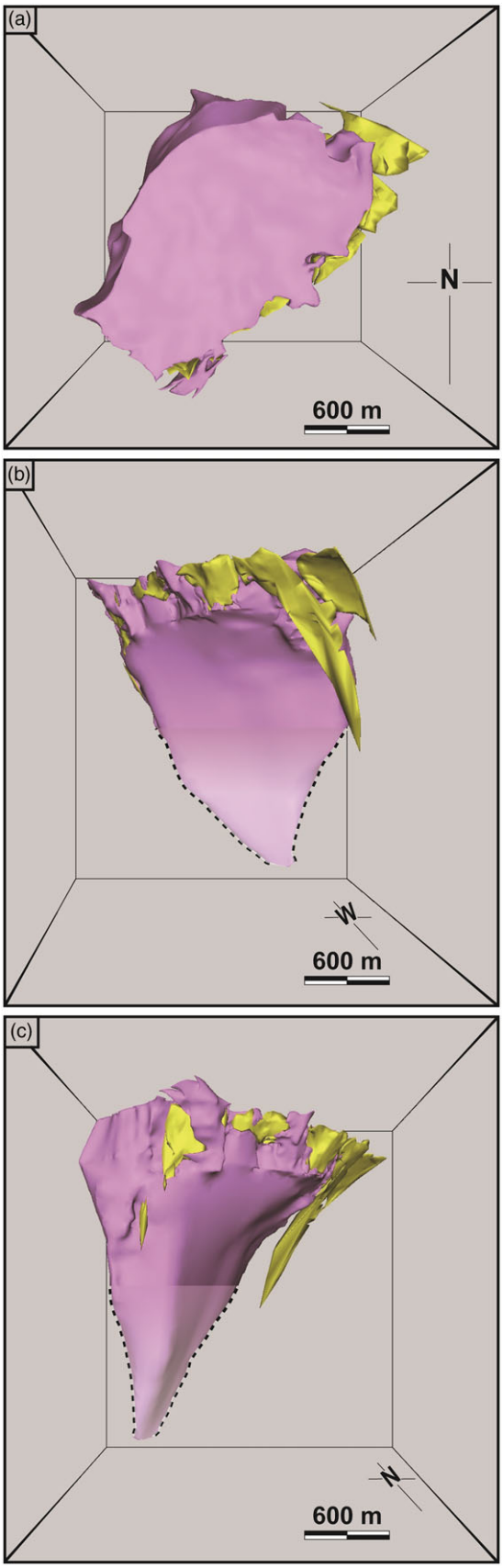

Fig. 9. (Colour online) 3D geometry of the TGS stock (pink) and its related ore bodies (yellow) reconstructed by the drilling and regional resistivity surveying data, view from the (a) top, (b) east and (c) south. Dashed line part represents the modelled geometry in the depth.

The Tongguanshan intrusion was considered as a stock and defined as a diapirically emplaced body in previous studies (Xu *et al.* 2004; Lei *et al.* 2010; Wu *et al.* 2010; Yang *et al.* 2015). Previous studies on the diapiric emplaced intrusions show that such a body is usually characterized by a spherical shape, compositional zonation, circular pattern of steep foliation and lineation, and the foliation and lineation parallel to the planar and linear fabrics developed in its aureole (e.g. Dixon, 1975; Cruden, 1990; He *et al.* 2009; del Potro *et al.* 2013). However, our AMS results reveal that the sites in the stock margin show a dominantly inwards-dipping magnetic foliation with the strike parallel to the stock boundary (i.e. sites TL02, TL04 and TL05 in Fig. 8). The most pronounced feature of these sites is that they are characterized by a sub-horizontal magnetic lineation (dip angle < 45°; Fig. 8; Table 2), which is contrary to the usually steep magnetic lineation pattern of the diapiric pluton revealed by previous studies (e.g. Cruden, 1990; He *et al.* 2009). We therefore consider that the one-time magma tank diapiric emplacement model seems incompatible with the Tongguanshan stock.

The remarkable feature of the Tongguanshan stock AMS result is the parallelism of the magnetic foliation and the NE–SW-trending fold–thrust belt of the country rock (Fig. 8), indicating that the emplacement of the Tongguanshan stock was either controlled by the NE–SW extended pre-emplacement structures of the country rocks, or the stock was constructed by NE–SW-striking dykes.

5.a.2. Space for magma emplacement

Previous geochemistry and geochronology studies of the Tongguanshan stock suggest that the stock has similar composition at the margin and in the centre. Zircon SHRIMP U–Pb dating of the Tongguanshan quartz–monzodiorite yields similar crystallization ages within the error bars – 139 ± 3, 139.5 ± 2.9 and 141.8 ± 1.0 Ma – suggesting that the duration of construction of the stock was relatively short (Du *et al.* 2004; Wang *et al.* 2004; Wu *et al.* 2010). The short duration is also supported by the small stock volume (*c.* 1.25 km^3) revealed by the 3D geometric modelling; as proposed by de Saint Blanquat *et al.* (2011), the emplacement duration has a linear relationship with the volume of intrusion. Considering that the regional tectonic strain rate is usually much lower than the magma supply rate (Price, 1975), the contribution of syn-magmatism regional tectonics to the creation of the emplacement space can be neglected. The NE–SW-striking and SE-dipping garnet- and magnetite-bearing veins developed in the eastern margin of the Tongguanshan stock, which correspond to the Early Cretaceous regional extension in the NW–SE direction (Fig. 3b, c; Wang *et al.* 2007; Li *et al.* 2009; Deng *et al.* 2011; Xie *et al.* 2012), cross-cut the NW-dipping magnetic foliation developed in the stock, suggesting that the regional extensional event occurred after the magma emplacement. As mentioned above, our field and thin-section observations also show that the stock is characterized by magmatic texture and fabrics developed in the country rocks before the magma emplacement (Figs 4, 6). We therefore believe that the Tongguanshan stock emplacement was possibly not influenced by the regional tectonic regime. Alternatively, the magma pressure from the accreted magma chamber may be considered as the principal space-creating force for magma emplacement.

The emplacement depth of the Tongguanshan stock is estimated at *c.* 3–5 km, that is, the brittle upper crust level (Du *et al.* 2004; Cao *et al.* 2009; Lei *et al.* 2010); the mechanical discontinuity interfaces in the country rocks are therefore preferable for the magma emplacement, and the re-arrangement of the country rocks

https://doi.org/10.1017/S001675682100056X Published online by Cambridge University Press

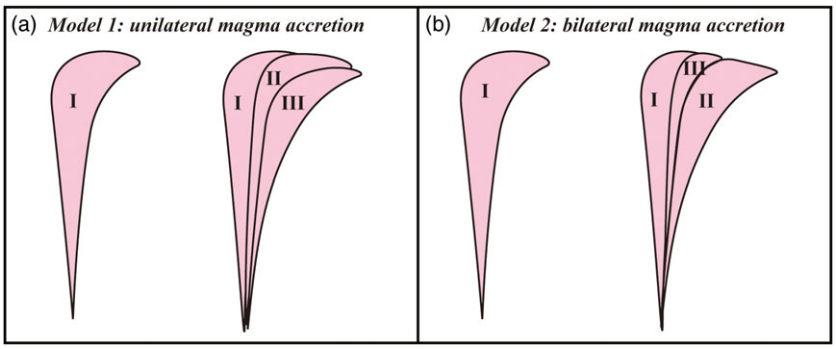

Fig. 10. (Colour online) Cross-sections through the conceptual model of the TGS stock in the E–W direction (not to scale). I, II and III represent the gradually emplaced magma pulses.

also partly accommodated the intrusions (e.g. Gudmundsson, 2011; Menand, 2011; Schofield *et al.* 2012). For example, the shouldering effect observed at the western margin of the Tongguanshan stock suggests the lateral movement behaviour of the country rock (Fig. 2). The stock–country-rock contact profiles in the east side revealed by the drilling data reveal that the dip angle of the contact surface gradually decreases from *c.* 65° in the south to *c.* 45° in the north (Fig. 5), indicating that the space for magma emplacement was partly accommodated by the downwards displacement of the country rocks.

Accordingly, we propose that the space for the emplacement of the Tongguanshan stock was mainly created by magma pressure from the magma chamber along the inherited regional structures in the country rocks, and partially associated with the lateral and downwards country rock displacement.

5.a.3. Emplacement mechanism of the Tongguanshan stock

The reconstructed 3D geometry of the Tongguanshan stock shows that the west contact surface is much steeper than the east contact surface and the root of stock is in the SW part of the stock (Fig. 9b, c), indicating that the magma emplacement was possibly initiated at the western stock margin. The crystal grain size in the stock shows a gradually fining trend from the centre to the east stock margin (Figs 2, 6). In addition, the strike of the magnetic foliation at sites TL02 and TL04 is parallel to the NW–SE-trending stock boundary, where the lower Permian strata are folded (Figs 5, 8), suggesting that the magma was accumulated at the pluton northern part. It therefore seems reasonable to assume that the magma emplacement was initiated at the southwestern part of the stock.

Site TL03 has the furthest distance to the stock margin and lowest degree of anisotropy value compared with other sites (Fig. 8), indicating that the magmatic fabric of site TL03 is mainly produced by magma emplacement. The understanding of the magnetic fabrics at site TL03 is therefore important to reconstruct the accretion process of the stock. Site TL03 is characterized by vertical NE–SW-striking magnetic foliations with variable plunges of magnetic lineation (Fig. 8). This is different from the inwards-dipping magnetic foliation and horizontal to sub-horizontal magnetic lineation in the stock margin, suggesting that site TL03 may be derived from different magma pulses with respect to other sites in the stock margin, instead of just a single magma intrusion. The relatively lower degree of anisotropy of site TL03 compared with sites TL02, TL04 and TL05 supports this idea (Fig. 7b). However, the accretion process is still not clear due to the lack of exposure in the western part of the Tongguanshan stock. We consider that there are two possibilities of forming the magnetic fabric of site TL03, and therefore two corresponding emplacement models were proposed. One is that site TL03 represents one of the magma pulses intruded along the NE–SW-extended pre-emplacement structures in the country rock with unilateral E-wards accretion trend (Model 1 in Fig. 10a). The other is that site TL03 belongs to the youngest magma pulse squeezed into the early emplaced magma, that is, bilateral magma accretion process (Model 2 in Fig. 10b). The ambient stress from earlier emplaced magma and country rocks therefore resulted in the NE–SW-extended magnetic foliation.

In summary, we conclude that the Tongguanshan stock was constructed by multiple magma pulses emplaced along the NE–SW-trending pre-emplacement structures in the country rock. The magma emplacement was initiated in the western part of the stock with either unilateral or bilateral magma accretion trend.

5.b. Influence of magma emplacement on the localization of related skarn type orebodies

The influence of magma emplacement on the related orebody localization mainly included the modification of the thermal fluid composition and pressure condition (e.g. Ray *et al.* 1995; Audétat *et al.* 2000; Vallance *et al.* 2003; Gerbault, 2012), the change of the circulation and accumulation of the hydrothermal fluid flow in the aureole (e.g. Boyce *et al.* 2003; Lu *et al.* 2003; Eldursi *et al.* 2009; Luan *et al.* 2014), and enhancement of the permeability and temperature gradients of the country rock (e.g. Nehlig, 1994; Matter *et al.* 2005; Gonnermann & Manga, 2009). Previous geochemical studies in the Tongguanshan orefield suggested that the origin of the hydrothermal fluid is mainly from the Tongguanshan stock (Yuan, 2002; Tian *et al.* 2005).

Our stock emplacement model suggests that the Tongguanshan stock was constructed by successively emplaced magma pulses along the NE–SW-striking fractures in the Tongguanshan anticline from west to east (Figs 11, 12). Consequently, the country rocks in the eastern side were heated and deformed by the successively emplaced magma arrivals. The variable inclination of the contact surface in the eastern side, the highly irregular stock–country-rock boundary and grain boundary migration recrystallization of the quartz–monzodiorite in the eastern margin (Fig. 6) also suggest that the country rocks on the eastern side experienced a stronger deformation than that on the western side (Fig. 11). The fracture of the country rocks may therefore be more developed in the eastern side, which may enhance the hydrothermal fluid and larger skarnization in the country rocks.

Recent studies show that the stock geometry, especially the curvature of the intrusion–country-rock contact surface, strongly controls the localization of orebodies (Cao *et al.* 2020); the curvature of the contact surface affects the distribution of the dilation zone around the pluton, where the fluid pressure drops and ore

https://doi.org/10.1017/S001675682100056X Published online by Cambridge University Press

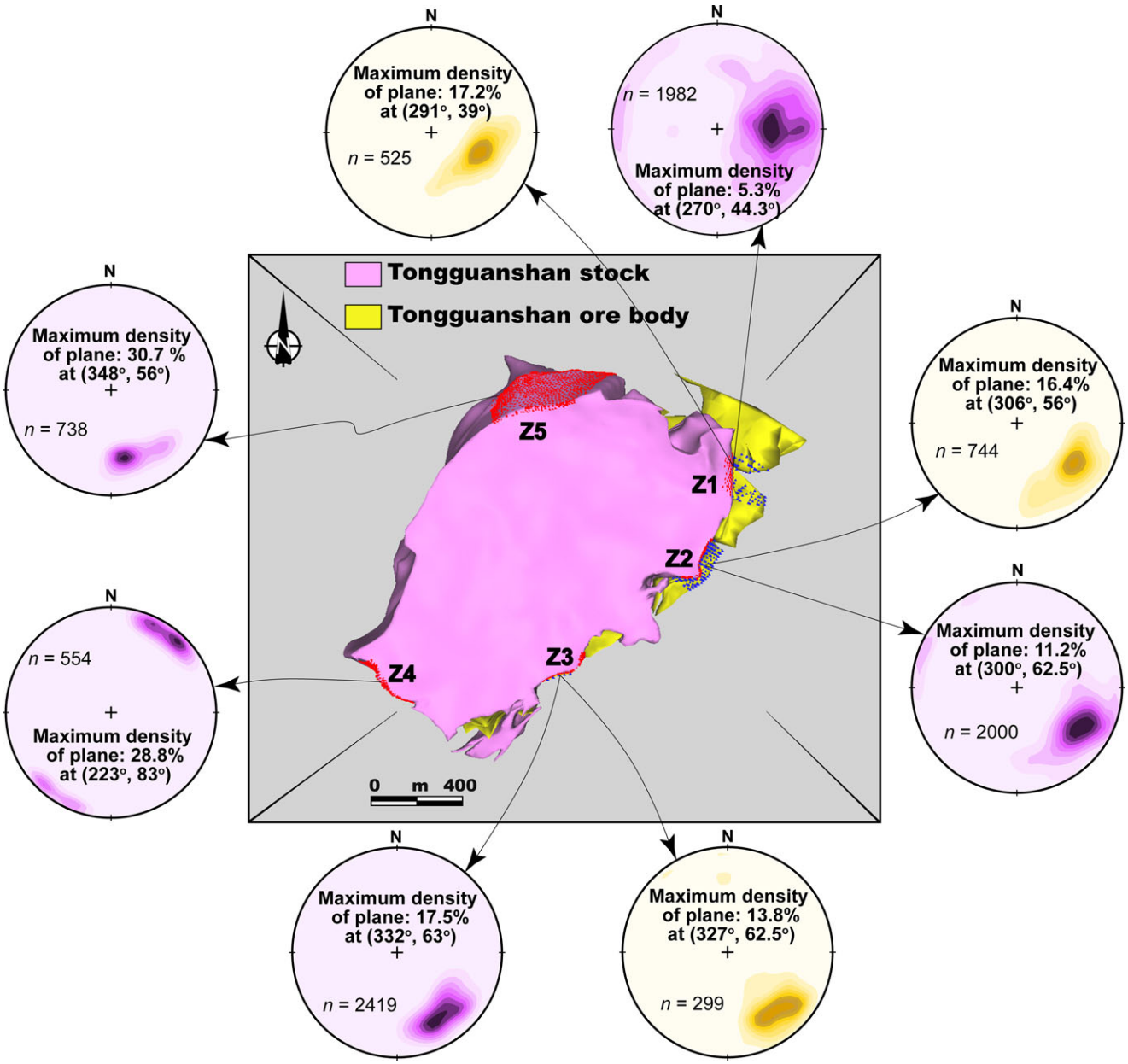

Fig. 11. (Colour online) Equal-area lower-hemisphere spherical projections of the stock–country-rock contact surface and its related skarn deposit. The pink and yellow spherical projections represent the stock-country rock surface and its related orebodies, respectively. The red and blue points in the image are the nodes of the Triangular Irregular Network (TIN) of analysed zone.

depositing occurs (Liu *et al.* 2012; Sun & Liu, 2014; Cao *et al.* 2020). To better understand the constraints of the stock geometry variance on its associated orebodies, we therefore chose five zones (Z1, Z2 and Z3, associated with copper skarn deposit, and Z4 and Z5, devoid of ore deposit) around the Tongguanshan stock contact with width and depth of *c.* 200 m (Fig. 11). From the comparative analysis of the variation of stock contact surface and extension of the orebodies along the contact surface, we can possibly correlate the stock geometry and ore deposits.

The equal-area projections of the contact surface of the stock in zones Z1, Z2 and Z3 show that the extension of the orebodies (yellow stereograms in Fig. 11) is parallel to the stock–country-rock contact surface, and the dip of the stock contact surface ranges over *c.* 45–65° (purple stereograms in Fig. 11). However, in zones Z4 and Z5, the dip of the contact surface is between 56° and 83°, which is statistically steeper than those in zones Z1, Z2 and Z3 (Fig. 11), but the strike of the contact boundary is oblique to the regional structures and no industrial mineral deposit was revealed in these zones. Furthermore, strong sericitization was observed in the quartz–monzodiorite along the cleavage, which is parallel to the strike of the magnetic foliation (Fig. 3c) and the long axis of crystal grain in the country rocks (Fig. 6d–f). The sericitization was related to the hydrothermal fluid flow during magma emplacement, suggesting that the hydrothermal fluid flow was also along the strike of the regional structures. Consequently, the genesis of the skarn-type ore deposit was mainly dependent upon the interaction between the stock-derived thermal fluid and the country rock. We therefore suggest that the parallelism among the strike of the contact surface, regional structures and direction of fluid flow facilitated the ore development.

https://doi.org/10.1017/S001675682100056X Published online by Cambridge University Press

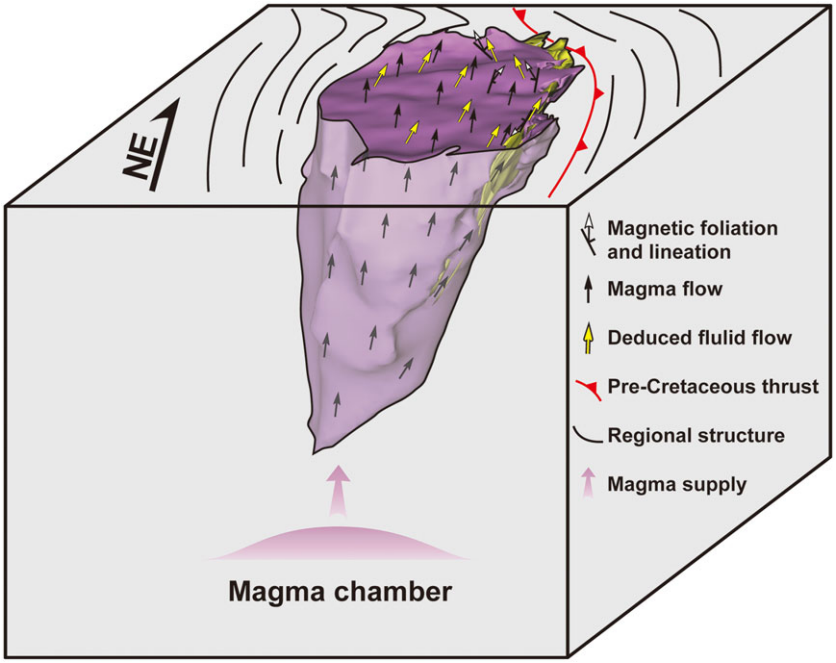

Fig. 12. (Colour online) Schematic magma emplacement and hydrothermal fluid flow pattern of the Tongguanshan stock (not to scale).

Generally, the lower the value of maximum density of stock contact surface, the more complex the curvature of the contact surface. Our study reveals that the value of maximum density of contact surface increased from Z1 to Z3 (5.3% to 17.5%), and almost doubled at Z4 and Z5 (28.8% to 30.7%, Fig. 11). However, the ore reservation decreased from Z1 to Z5, indicating that the curvature of the contact surface is positively correlated with the ore reservation. From a comparative analysis of these five zones, we consider that the curvature of the contact surface is equivalent to the distribution of the dilation zone, important ore-controlling factors in an intrusion-related ore deposit.

We therefore argue that the emplacement process, that is, the stock–country-rock contact surface geometry, emplacement depth and magma accretion process, may be an essential ore-controlling factor for the ore deposit localization. This idea can be used to guide further prospecting for large-scaled intrusion-related deposits, which are usually constructed from numerous magma batches. However, to obtain a more comprehensive understanding of the magma emplacement and its effect on the related mineralization process, detailed 3D emplacement process studies on a developed mining area are needed.

6. Conclusions

From our field and thin-section observations, AMS, and 3D geometry studies of the Tongguanshan stock and its related orebodies, we make the following conclusions.

(1) The Tongguanshan stock is composed of macroscopically isotropic quartz–monzodiorite with a 'tongue-like' geometry and a sharp wedge of *c.* 2 km depth in the western side of the Tongguanshan stock.
(2) The magma emplacement was initiated in the western side of the Tongguanshan stock, and the magma ascended along inherited NE–SW-striking fractures developed in the Tongguanshan anticline. The successive magma arrivals were either unilaterally accreted to the east side of the stock or bilaterally accreted by a succession of NE–SW striking magma pulses.
(3) The strike, dip angle and curvature situation of the stock–country-rock contact surface, which may affect the water–rock reaction process and distribution of the dilation zone, are important ore-controlling factors.

Acknowledgements. We thank Xiao Fuquan, Wu Shuo, Li Min and Chen Bin for their help with sample collection, and Hu Xuzhi (the Paleomagnetism Laboratory of the Nanjing University) and Tao Shuai (Northwest University) for their help with AMS measurements. We also thank Carl Stevenson and one anonymous reviewer for their constructive comments and suggestions. The provision of the drilling data from the Tongling Nonferrous Metals Group Holdings Company was greatly appreciated. Our study received financial support from the National Natural Science Foundation of China (grant nos 41372338 and 41772351).

Conflict of interest. None.

References

Audétat A, Günther D and Heinrich CA (2000) Causes for large-scale metal zonation around mineralized plutons: fluid inclusion LA-ICP-MS evidence from the Mole Granite, Australia. *Economic Geology* **95**, 1563–81. doi: 10.2113/gsecongeo.95.8.1563

Baker T, Van Achterberg E, Ryan CG and Lang JR (2004) Composition and evolution of ore fluids in a magmatic-hydrothermal skarn deposit. *Geology* **32**, 117–20.

Boyce AJ, Fulignati P and Sbrana A (2003) Deep hydrothermal circulation in a granite intrusion beneath Larderello geothermal area (Italy): constraints from mineralogy, fluid inclusions and stable isotopes. *Journal of Volcanology and Geothermal Research* **126**, 243–62. doi: 10.1016/S0377-0273(03)00150-1

Cao W, Liu L, Liu H and Lai F (2020) Investigating the irregular localization of skarn orebodies by computational modeling in the Fenghuangshan Ore Field, Tongling District, Anhui Province, China. *Natural Resources Research* **29**, 2967–88. doi: 10.1007/s11053-020-09655-x

Cao Y, Du Y-S, Pang Z-S, Li S-T, Zhang J and Zhang Z-C (2009) Underplating and assimilation-fractional crystallization of Mesozoic intrusions in the Tongling area, Anhui Province, East China: evidence from xenoliths and

host plutons. *International Geology Review* **51**, 542–55. doi: 10.1080/00206810902837206

Chang YF, Liu XP and Wu YC (1991) *The Copper–Iron Belt of the Middle and Lower Reaches of the Changjiang River*. Beijing: Geological Publishing House, 379 p.

Chen Y and Nabelek PI (2017) The influences of incremental pluton growth on magma crystallinity and aureole rheology: numerical modeling of growth of the Papoose Flat pluton, California. *Contributions to Mineralogy and Petrology* **172**, 89. doi: 10.1007/s00410-017-1405-6

Cruden AR (1990) Flow and fabric development during the diapiric rise of magma. *Journal of Geology* **98**, 681–98.

de Saint Blanquat M, Horsman E, Habert G, Morgan S, Vanderhaeghe O, Law R and Tikoff B (2011) Multiscale magmatic cyclicity, duration of pluton construction, and the paradoxical relationship between tectonism and plutonism in continental arcs. *Tectonophysics* **500**, 20–33. doi: 10.1016/j.tecto.2009.12.009

del Potro R, Díez M, Blundy J, Camacho AG and Gottsmann J (2013) Diapiric ascent of silicic magma beneath the Bolivian Altiplano. *Geophysical Research Letters* **40**, 2044–48. doi: 10.1002/grl.50493

Deng J, Wang Q, Huang D, Wan L, Yang L and Gao B (2006) Transport network and flow mechanism of shallow ore-bearing magma in Tongling ore cluster area. *Science in China Series D* **49**, 397–407. doi: 10.1007/s11430-006-0397-2

Deng J, Wang Q, Xiao C, Yang L, Liu H, Gong Q and Zhang J (2011) Tectonic-magmatic-metallogenic system, Tongling ore cluster region, Anhui Province, China. *International Geology Review* **53**, 449–76.

Dilles JH and Proffett JM (1995) Metallogenesis of the Yerington batholith, Nevada. In *Porphyry Copper Deposits of the American Cordillera* (eds FW Pierce and JG Bolm), pp. 306–15. Tucson: Arizona Geological Society Digest, vol. 20.

Dines HG (1956) *The Metalliferous Mining Region of South-West England*, vol. **2**. London: HMSO.

Dixon JM (1975) Finite strain and progressive deformation in models of diapiric structures. *Tectonophysics* **28**, 89–124. doi: 10.1016/0040-1951(75)90060-8

Du YS, Li ST, Cao Y, Qin XL and Lou Y (2007) UAFC-related origin of the Late Jurassic to Early Cretaceous intrusions in the Tongguanshan ore field, Tongling, Anhui Province: East China. *Geoscience* **21**, 71–77 (in Chinese with English abstract).

Du YS, Qin XL and Tian SH (2004) Mesozoic magmatic to hydrothermal process in the Tongguanshan ore field, Tongling, Anhui province, China: evidence from xenoliths and their hosts. *Acta Petrologica Sinica* **20**, 339–50 (in Chinese with English abstract).

Dunlop D (1974) Thermal enhancement of magnetic susceptibility. *Journal of Geophysics* **40**, 439–51.

Einaudi MT, Meinert LD and Newberry RJ (1981) Skarn deposits. In *Economic Geology: 75th Anniversary Volume* (ed. BJ Skinner), pp. 317–91. Littleton, CO: Society of Economic Geologists.

Eldursi K, Branquet Y, Guillou-Frottier L and Marcoux E (2009) Numerical investigation of transient hydrothermal processes around intrusions: heat-transfer and fluid-circulation controlled mineralization patterns. *Earth and Planetary Science Letters* **288**, 70–83. doi: 10.1016/j.epsl.2009.09.009

Faure M, Shu LS, Wang B, Charvet J, Choulet F and Monie P (2009) Intracontinental subduction: a possible mechanism for the Early Palaeozoic Orogen of SE China. Terra Nova **21**, 360–68.

Feng Z, Wang C, Zhang M and Liang J (2012) Unusually dumbbell-shaped Guposhan–Huashan twin granite plutons in Nanling Range of south China: Discussion on their incremental emplacement and growth mechanism. *Journal of Asian Earth Sciences* **48**, 9–23. doi: 10.1016/j.jseaes.2011.12.022

Ferry JM and Dipple G (1992) Models for coupled fluid flow, mineral reaction, and isotopic alteration during contact metamorphism: the Notch Peak aureole, Utah. *American Mineralogist* **77**, 5–6.

Galadí-Enríquez E, Galindo-Zaldívar J, Simancas F and Expósito I (2003) Diapiric emplacement in the upper crust of a granitic body: the La Bazana granite (SW Spain). *Tectonophysics* **361**, 83–96. doi: 10.1016/S0040-1951(02)00562-0

Geological Team of Anhui Bureau of Geology and Mineral Resources (1989) No. 321 1:50 000 geological map and its notations of Tongling area (in Chinese). Hefei: Anhui Bureau of Geology and Mineral Resources.

Gerbault M (2012) Pressure conditions for shear and tensile failure around a circular magma chamber; insight from elasto-plastic modelling. In *Faulting, Fracturing and Igneous Intrusion in the Earth's Crust* (eds D Healy, RWH Butler, ZK Shipton and RH Sibson), pp. 111–30. Geological Society of London, Special Publication no. 367.

Gerdes ML, Baumgartner LP and Person M (1998) Convective fluid flow through heterogeneous country rocks during contact metamorphism. *Journal of Geophysical Research: Solid Earth* **103**, 23983.

Gonnermann HM, Giachetti T, Fliedner C, Nguyen CT, Houghton BF, Crozier JA and Carey RJ (2017) Permeability during magma expansion and compaction. *Journal of Geophysical Research: Solid Earth* **122**, 9825–48.

Gonnermann HM and Manga M (2009) Magma ascent in the volcanic conduit. In *Modeling Volcanic Processes: The Physics and Mathematics of Volcanism* (eds S Fagents, TKP Gregg and RMC Lopes), pp. 55–84. New York: Cambridge University Press.

Gudmundsson A (2011) Deflection of dykes into sills at discontinuities and magma-chamber formation. *Tectonophysics* **500**, 50–64. doi: 10.1016/j.tecto.2009.10.015

Hacker BR, Ratschbacher L and Liou JG (2004) Subduction, collision, and exhumation in the Qinling-Dabie Orogen. *Journal of the Geological Society of London* **226**, 157–75.

He B, Xu YG and Paterson S (2009) Magmatic diapirism of the Fangshan pluton, southwest of Beijing, China. *Journal of Structural Geology* **31**, 615–26.

Heinrich CA (2005) The physical and chemical evolution of low-salinity magmatic fluids at the porphyry to epithermal transition: a thermodynamic study. *Mineralium Deposita* **39**, 864–89. doi: 10.1007/s00126-004-0461-9

Ji W, Chen Y, Chen K, Wei W, Faure M and Lin W (2018) Multiple emplacement and exhumation history of the Late Mesozoic Dayunshan-Mufushan Batholith in southeast China and its tectonic significance: 2. Magnetic fabrics and gravity survey. *Journal of Geophysical Research: Solid Earth* **123**, 711–31. doi: 10.1002/2017jb014598

Kratinová Z, Závada P, Hrouda F and Schulmann K (2006) Non-scaled analogue modelling of AMS development during viscous flow: a simulation on diapir-like structures. *Tectonophysics* **418**, 51–61. doi: 10.1016/j.tecto.2005.12.013

Lei M, Wu CL, Gao QM, Guo HP, Liu LG, Guo XY, Gao YH, Chen Q and Qin HP (2010) Petrogenesis of intermediate-acid intrusive rocks and enclaves in Tongling area and the application of mineral thermobarometry. *Acta Petrologica et Mineralogica* **29**, 271–88 (in Chinese with English abstract).

Li JW, Pei RF, Zhang DQ, Mei YX, Zang WS, Meng GX, Zeng PS, Li TJ and Di YJ (2007) Geochemical characteristics of the Yanshannian intermediate-acid intrusive rocks in the Tongling mineralization concentration area, Anhui province, and their geological implications. *Acta Geoscientica Sinica* **28**, 11–22 (in Chinese with English abstract).

Li JW, Zhao XF, Zhou MF, Ma CQ, Sergio de Souza Z and Vasconcelos P (2009) Late Mesozoic magmatism from Daye region, eastern China: U–Pb ages, petrogenesis, and geodynamic implications. *Contributions to Mineralogy and Petrology* **157**, 383–409.

Li Y, Li Q-L and Yang J-H (2019) Tracing water-rock interaction in carbonate replacement deposits: a SIMS pyrite S-Pb isotope perspective from the Chinese Xinqiao system. *Ore Geology Reviews* **107**, 248–57. doi: 10.1016/j.oregeorev.2019.02.022

Liu H, Chen Y, Wang B, Faure M, Erdmann S, Martelet G, Scaillet B and Huang F (2020) Role of inherited structure on granite emplacement: an example from the Late Jurassic Shibei pluton in the Wuyishan area (South China) and its tectonic implications. *Tectonophysics* **779**, 228394. doi: 10.1016/j.tecto.2020.228394

Liu H, Martelet G, Wang B, Erdmann S, Chen Y, Faure M, Huang F, Scaillet B, Le Breton N, Shu L and Wang R (2018a) Incremental Emplacement of the Late Jurassic midcrustal, lopolith-like Qitianling Pluton, South China, revealed by AMS and Bouguer gravity data. *Journal of Geophysical Research: Solid Earth*, **123**, 9249–68. doi: 10.1029/2018JB015761

Liu L, Zhao Y and Sun T (2012) 3D computational shape- and cooling process-modeling of magmatic intrusion and its implication for genesis and exploration of intrusion-related ore deposits: an example from the Yueshan intrusion in Anqing, China. *Tectonophysics* **526–529**, 110–23. doi: 10.1016/j.tecto.2011.09.006

Liu L, Zhao Y and Zhao C (2010) Coupled geodynamics in the formation of Cu skarn deposits in the Tongling–Anqing district, China: computational modeling and implications for exploration. *Journal of Geochemical Exploration* **106**, 146–55.

Liu LM, Sun T and Zhou RC (2014) Epigenetic genesis and magmatic intrusion's control on the Dongguashan stratabound Cu–Au deposit, Tongling, China: evidence from field geology and numerical modeling. *Journal of Geochemical Exploration* **144**, 97–114.

Liu Z-F, Shao, Y-J, Wang C and Liu Q-Q (2018b) Genesis of the Dongguashan skarn Cu-(Au) deposit in Tongling, Eastern China: evidence from fluid inclusions and H-O-S-Pb isotopes. *Ore Geology Reviews* **104**, 462–76. doi: 10.1016/j.oregeorev.2018.11.021

Lu H-Z, Liu Y, Wang C, Xu Y and Li H (2003) Mineralization and fluid inclusion study of the Shizhuyuan W-Sn-Bi-Mo-F skarn deposit, Hunan Province, China. *Economic Geology* **98**, 955–74.

Lü Q, Hou Z and Zhao JH (2003) Deep seismic reflection profiling reveals complex crustal structure of Tongling ore district. *Science in China* **33**, 442–49.

Luan Y, Song X-Y, Chen L-M, Zheng W-Q, Zhang X-Q, Yu S-Y, She YW, Tian XL and Ran Q-Y (2014) Key factors controlling the accumulation of the Fe–Ti oxides in the Hongge layered intrusion in the Emeishan Large Igneous Province, SW China. *Ore Geology Reviews* **57**, 518–38. doi: 10.1016/j.oregeorev.2013.08.010

Mao J, Xie G, Duan C, Pirajno F, Ishiyama D and Chen Y (2011) A tectono-genetic model for porphyry–skarn–stratabound Cu–Au–Mo–Fe and magnetite–apatite deposits along the Middle–Lower Yangtze River Valley, Eastern China. *Ore Geology Reviews* **43**, 294–314. doi: 10.1016/j.oregeorev.2011.07.010

Matter JM, Goldberg DS, Morin RH and Stute M (2005) Contact zone permeability at intrusion boundaries: new results from hydraulic testing and geophysical logging in the Newark Rift Basin, New York, USA. *Hydrogeology Journal* **14**, 689. doi: 10.1007/s10040-005-0456-3

Meinert LD (2005) World skarn deposits. In *Economic Geology: 100th Anniversary Volume* (eds JW Hedenquist, JFH Thompson, RJ Goldfarb and JP Richards), pp. 299–336. Littleton, CO: Society of Economic Geologists.

Menand T (2008) The mechanics and dynamics of sills in layered elastic rocks and their implications for the growth of laccoliths and other igneous complexes. *Earth & Planetary Science Letters* **267**, 93–99.

Menand T (2011) Physical controls and depth of emplacement of igneous bodies: a review. *Tectonophysics* **500**, 11–19. doi: 10.1016/j.tecto.2009.10.016

Meng YF, Yang ZS, Zeng PS, Xu WY and Wang XC (2004) Tentative temporal constraints of ore-forming fluid systems in Tongling Metallogenic Province. *Mineral Deposits* **23**, 271–80 (in Chinese with English abstract).

Nehlig P (1994) Fracture and permeability analysis in magma-hydrothermal transition zones in the Samail ophiolite (Oman). *Journal of Geophysical Research: Solid Earth* **99**, 589–601. doi: 10.1029/93jb02569

Pan Y and Dong P (1999) The Lower Changjiang (Yangzi/Yangtze River) metallogenic belt, east central China: intrusion- and wall rock-hosted Cu–Fe–Au, Mo, Zn, Pb, Ag deposits. *Ore Geology Reviews* **15**, 177–242. doi: 10.1016/S0169-1368(99)00022-0

Paterson SR, Okaya D, Memeti V, Economos R and Miller RB (2011) Magma addition and flux calculations of incrementally constructed magma chambers in continental margin arcs: combined field, geochronologic, and thermal modeling studies. *Geosphere* **7**, 1439–68.

Price NJ (1975) Rates of deformation. *Journal of the Geological Society* **131**, 553–75.

Ray GE, Webster ICL and Ettlinger AD (1995) The distribution of skarns in British Columbia and the chemistry and ages of their related plutonic rocks. *Economic Geology* **90**, 920–37.

Richards J P (2003) Tectono-magmatic precursors for porphyry Cu-(Mo-Au) deposit formation. *Economic Geology* **98**, 1515–33.

Rochette P, Jackson M and Aubourg C (1992) Rock magnetism and the interpretation of anisotropy of magnetic susceptibility. *Reviews of Geophysics* **30**, 209–26. doi: 10.1029/92RG00733

Scaillet B, Holtz F, Pichavant M and Schmidt M (1996) Viscosity of Himalayan leucogranites: Implications for mechanisms of granitic magma ascent. *Journal of Geophysical Research: Solid Earth* **101**, 27691–99. doi: 10.1029/96jb01631

Schofield NJ, Brown DJ, Magee C and Stevenson CT (2012) Sill morphology and comparison of brittle and non-brittle emplacement mechanisms. *Journal of the Geological Society* **169**, 127–41. doi: 10.1144/0016-76492011-078

Seedorf E, Dilles JH, Proffett JMJ, Einaudi MR, Zurcher L, Stavast WJA, Johnson DA and Barton MD (2005) Porphyry deposits: characteristics and origin of hypogene features. In *Economic Geology: 100th Anniversary Volume* (eds JW Hedenquist, JFH Thompson, RJ Goldfarb and JP Richards), pp. 251–98. Littleton, CO: Society of Economic Geologists.

Shu LS, Faure M, Yu JH and Jahn BM (2011) Geochronological and geochemical features of the Cathaysia block (South China): new evidence for the Neoproterozoic breakup of Rodinia. *Precambrian Research* **187**, 263–76.

Sial AN, Bettencourt JS, De Campos CP and Ferreira VP (eds) (2011) *Granite-Related Ore Deposits*. Geological Society of London, Special Publication no. 350.

Sun T and Liu L (2014) Delineating the complexity of Cu–Mo mineralization in a porphyry intrusion by computational and fractal modeling: a case study of the Chehugou deposit in the Chifeng district, Inner Mongolia, China. *Journal of Geochemical Exploration* **144**, 128–43.

Tahiri A, Simancas JF, Azor A, Galindo-Zaldívar J, González Lodeiro F, El Hadi H, Poyatos DM and Ruiz-Constán A (2007) Emplacement of ellipsoid-shaped (diapiric?) granite: Structural and gravimetric analysis of the Oulmès granite (Variscan Meseta, Morocco). *Journal of African Earth Sciences* **48**, 301–13. doi: 10.1016/j.jafrearsci.2007.04.005

Tang ZL (2002) Magmatic ore deposits in small rock body in China. *Engineering Science* **4**, 9–12 (in Chinese with English Abstract).

Thompson JFH, Sillitoe RH, Baker T, Lang JR and Mortensen JK (1999) Intrusion-related gold deposits associated with tungsten-tin provinces. *Mineralium Deposita* **34**, 323–34. doi: 10.1007/s001260050207

Tian SH, Ding TP, Hou ZQ, Yang ZS, Xie YL, Wang YB and Wang XC (2005) REE and stable isotope geochemistry of the Xiaotongguanshan copper deposit, Tongling, Anhui. *Geology in China* **32**, 604–12 (in Chinese with English Abstract).

Tibaldi A, Rovida A and Corazzato C (2007) Late Quaternary kinematics, slip-rate and segmentation of a major Cordillera-parallel transcurrent fault: The Cayambe-Afiladores-Sibundoy system, NW South America. *Journal of Structural Geology* **29**, 664–80. doi: 10.1016/j.jsg.2006.11.008

Vallance J, Cathelineau M, Boiron MC, Fourcade S, Shepherd TJ and Naden J (2003) Fluid-rock interactions and the role of late Hercynian aplite intrusion in the genesis of the Castromil gold deposit, northern Portugal. *Chemical Geology* **194**, 201–24.

Wang J and Li ZX (2003) History of Neoproterozoic rift basins in South China: implications for Rodinia break-up. *Precambrian Research* **122**, 141–58.

Wang Q, Wyman DA, Xu JF, Zhao ZH, Jian P and Zi F (2007) Partial melting of thickened or delaminated lower crust in the middle of Eastern China: implications for Cu–Au mineralization. *Journal of Geology* **115**, 149–61.

Wang YB, Zeng PS, Yang ZS, Meng YF and Tian SH (2004) SHRIMP U-Pb geochronology of Xiaotongguanshan quartz-dioritic intrusions in the Tongling district and its petrogenetic implications. *Acta Petrologica et Mineralogica* **23**, 298–304 (in Chinese with English Abstract).

Wei W, Chen Y, Faure M, Martelet G, Lin W, Wang Q, Yan Q and Hou Q (2016) An early extensional event of the South China Block during the Late Mesozoic recorded by the emplacement of the Late Jurassic syntectonic Hengshan Composite Granitic Massif (Hunan, SE China). *Tectonophysics* **672–673**, 50–67. doi: 10.1016/j.tecto.2016.01.028

Wei W, Martelet G, Le Breton N, Shi Y, Faure M, Chen Y, Hou Q, Lin W and Wang Q (2014) A multidisciplinary study of the emplacement mechanism of the Qingyang–Jiuhua massif in Southeast China and its tectonic bearings. Part II: amphibole geobarometry and gravity modeling. *Journal of Asian Earth Sciences* **86**, 94–105. doi: 10.1016/j.jseaes.2013.09.021

Wu C, Dong S, Robinson PT, Frost BR, Gao Y, Lei M, Chen Q and Qin H (2013) Petrogenesis of high-K, calc-alkaline and shoshonitic intrusive rocks in the Tongling area, Anhui Province (eastern China), and their tectonic implications. *Geological Society of America Bulletin* **126**, 78–102. doi: 10.1130/b30613.1

Wu CL, Gao QM, Guo HP, Guo XY, Liu LG, Gao YH, Lei M, Qin HP and Chen QL (2010) Zircon SHRIMP dating of intrusive rocks from the Tongguanshan ore-field in Tongling, Anhui, China. *Acta Geologica Sinica* **84**, 1746–58 (in Chinese with English abstract).

Xie J, Yang X, Sun W and Du J (2012) Early Cretaceous dioritic rocks in the Tongling region, eastern China: Implications for the tectonic settings. *Lithos* **150**, 49–61. doi: 10.1016/j.lithos.2012.05.008

Xie JC, Yang XY, Du JG and Sun WD (2008) Zircon U-Pb geochronology of the Mesozoic intrusive rocks in the Tongling region: implications for copper-gold mineralization. *Acta Petrologica Sinica* **24**, 1782–800 (in Chinese with English Abstract).

Xiong X, Zhu L, Zhang G, Guo A, Zheng J and Jiang H (2019) Origin of the Xiaohekou skarn copper deposit and related granitoids in the Zha-Shan ore cluster area, South Qinling, China. *Ore Geology Reviews* 114, 103143. doi: 10.1016/j.oregeorev.2019.103143

Xu XS, Fun QC, O'Reilly SY, Jiang SY, Griffin WL, Wang RC and Qiu JS (2004) Zircon U-Pb dating of the quartz diorite and its enclaves in Tongguanshan, Anhui Province: discussion on the petrologic genesis: *Chinese Science Bulletin* **49**, 1883–91. doi: 10.1360/04wd0137

Xu ZQ, Zeng LS and Liu FL (2006) Polyphase subduction and exhumation of the Sulu high-pressure-ultrahigh-pressure metamorphic terrane. *Geological Society of America, Special Paper* **403**, 93–113.

Yang YC, Du YS, Li MS, Li MX and Cao QY (2015) Mineralogical characteristic of the Tian'ebaodan in the Tongling area, Anhui quartz diorite province and its geological significance. *Journal of Mineral Petrol* **35**, 51–58 (in Chinese with English abstract).

Yuan XM (2002) A tentative discussion on the copper and gold metallogenic model of the Tongguanshan Orefield. *Acta Geoscientia Sinica* **23**, 541–46 (in Chinese with English abstract).

Zhang D, Liu W, Wu G, Li D, Di Y, Zang W and Huang H (2008) Magnetic fabric and emplacement of the Fenghuangshan Pluton, Tongling, Anhui Province, East-Central China. *International Geology Review* **50**, 994–1007. doi: 10.2747/0020-6814.50.11.994